Electronic Supplementary Information for

A Cu hollow fiber with coaxially grown Bi nanosheet arrays as an integrated gas-penetrable electrode enables high-current-density and durable formate electrosynthesis

Zhe Meng,[a,b,c] Fang Wang,[a,b,c] Zhengguo Zhang,[a,b,c] Shixiong Min*[a,b,c]

[a] *School of Chemistry and Chemical Engineering, North Minzu University, Yinchuan, 750021, P. R. China. E-mail: sxmin@nun.edu.cn*

[b] *Ningxia Key Laboratory of Solar Chemical Conversion Technology, North Minzu University, Yinchuan 750021, P. R. China.*

[c] *Key Laboratory of Chemical Engineering and Technology, State Ethnic Affairs Commission, North Minzu University, Yinchuan, 750021, P. R. China.*

1. Experimental

1.1 Chemicals and materials

All chemicals were used as received without further purification. Cu powder (99.9%, 1 μm) was purchased from Zhongmai Metal Materials Co., Ltd. Polyetherimide (PEI，molecular weight: 628.62 Da) was purchased from Saudi Basic Industries Corporation (SABIC). N-methyl-2-pyrrolidone (NMP, ≥99.0%) and potassium bicarbonate ($KHCO_3$, ≥99.5%) was purchased from Shanghai Titan Scientific Co., Ltd. Bismuth chloride ($BiCl_3$, ≥98%) and concentrated hydrochloric acid (HCl, 36~38%) was purchased from Sinopharm Chemical Reagent Co., Ltd. Dimethyl sulfoxide (DMSO, ≥99.5%) and anhydrous ethanol (C_2H_5OH, ≥99.7%) was purchased from Tianjin Damao Co., Ltd. The high-purity carbon dioxide (CO_2, 99.999%), nitrogen (N_2, 99.999%), and argon (Ar, 99.999%) was purchased from Jinghua Industrial Gas Co., Ltd. Nafion 117 membrane was purchased from by Alfa Aesar Chemical Co., Ltd. Ultrapure water (18.2 MΩ cm) was obtained from a water purification system (Hitech ECO-S15).

1.2 Catalysts preparation

1.2.1 Fabrication of Cu hollow fiber (Cu HF)

Cu HF was fabricated according to a previously reported combined phase-inversion/sintering process.[1] In brief, 5 g of PEI powder was first added into 15 g of NMP solution, followed by heating treatment at 80 °C for 8 h to obtain a transparent solution, to which 30 g of Cu powder was then added. The as-obtained mixture was further subjected to ball milling (300 rpm) for 3 h to form a homogeneous slurry. After cooling to room temperature, the slurry was vacuumized (1 mbar) for 12 h to remove the bubbles and obtain a casting solution. Next, the casting solution was extruded through a spinning machine and shaped in a water bath *via* the phase-inversion process.

After spinning, the as-formed tubes were kept in a water bath for 24 h to eliminate the NMP, followed by stretching and drying for 48 h to obtain a Cu HF precursor. The Cu HF precursor was cut into 6 cm in length and then was calcined in an 21% O_2 (N_2 balanced) flow (150 mL·min^{-1}) at 600 °C with a heating rate of 1 °C·min^{-1} for 6 h to remove PEI. After being naturally cooled to room temperature, the calcined Cu HF precursor was then reduced in a 10% H_2 (Ar balanced) flow (100 mL·min^{-1}) at 500 °C with a heating rate of 1 °C·min^{-1} for 3 h to obtain Cu HF.

1.2.2 Fabrication of Bi NSAs@Cu HF electrodes

The Bi NSAs@Cu HF electrodes were fabricated *via* the well-established galvanic replacement reaction (GRR).[2] The Cu HF was first washed with diluted HCl (1 M) for 10 min to remove the native oxide layer, then washed with deionized water and ethanol in turn, and finally dried in a N_2 flow at room temperature. Afterward, the clean Cu HF (2.5 cm) was immersed in 40 mL of DMSO solution containing $BiCl_3$ (20 μM) for variable amounts of time (1, 3, 6, and 9 h). The obtained Bi NSAs@Cu HF electrodes were rinsed with ethanol several times and dried under N_2 flow at room temperature.

1.3 Characterization

X-ray diffraction (XRD) patterns were analyzed in the 2θ range of 5~80° with a scanning rate of 10° min^{-1} using a Rigaku Smartlab diffractometer with Cu *K*α radiation, operating at 40 kV and 40 mA. Scanning electron microscopy (SEM) images and energy X-ray spectrometer (EDX) were taken with a SIGMA 500 scanning electron microscope. Transmission electron microscopy (TEM) images were taken with a FEI Talos F200x field emission transmission electron microscope. X-ray photoelectron spectroscopy (XPS) measurements of the samples were performed on a Thermo Fisher Escalab-250Xi electron spectrometer using an Al Kα X-ray source. All spectra were calibrated according to the C 1s binding energy at 284.8 eV. The atomic force

microscopy (AFM) images were taken with Bruker Dimension Icon atomic force microscopy, and the scanning range was 2×2 μm. Mechanical properties were estimated on a universal test machine (HZ-1003B, China). The stress-strain curves of the Cu HF were acquired at a stretch rate of 50 mm·min^{-1} until breaking.

1.4 Electrocatalytic CO_2 reduction experiments in an H-type cell

All the electrochemical experiments were conducted in an H-type electrochemical cell separated by a Nafion 117 membrane with a potentiostat (CS350M; Corrtest Instruments). A Pt mesh and a saturated Ag/AgCl electrode were used as the counter electrode and reference electrode, respectively. A 0.5 M $KHCO_3$ solution was used as the supporting electrolyte. The working electrode was prepared by sticking HF tube (Cu HF or Bi NSAs@Cu HF) into a Cu tube using conductive silver adhesive, while the end of the HF tube as well as the joints between the HF tube and Cu tube were sealed with nonconductive epoxy. The Cu tube was then connected to one inlet for gas flow in. All potentials were measured against a saturated Ag/AgCl electrode reference electrode and converted to the RHE reference after iR_s compensation using E (*vs.* RHE)=E (*vs.* Ag/AgCl)+0.655 V-iR_s.

Liner sweep voltammetry (LSV) measurements were carried out in Ar- or CO_2-saturated 0.5 M $KHCO_3$ solution at a scan rate of 10 mV s^{-1}. Electrical double layer capacitances of the electrodes were determined by performing cyclic voltammetry (CV) measurements in a non-faradaic region (0.16~0.26 V) in Ar bubbling 0.5 M $KHCO_3$ solution. The electrochemical impedance spectroscopy (EIS) measurements were performed in a frequency range from 0.01 Hz to 100 kHz at a voltage amplitude of 5 mV.

For the bulk CO_2 reduction at fixed applied potential, the gas effluent from the cathodic compartment was delivered directly to the sampling loop of an on-line pre-

calibrated gas chromatograph (PANNA GC-A91 plus) equipped with a thermal conductivity detector (TCD) and a flame ionization detector (FID). The Faradaic efficiency (FE) for the gaseous products were calculated based on the following Equation (1):

$$FE_i\ (\%) = \frac{Z_i \times G \times V_i \times t \times p_0 \times F \times 10^{-3}}{Q_{total} \times R \times T_0} \times 100\% \qquad (1)$$

where Z is the number of electrons transferred; G is volumetric outlet flow rate; V_i is the volume ratio of gas product i; t is reaction time (min); and p_0 is the atmospheric pressure (101.3 kPa), T_0 is the reaction temperature (298.15 K), F is faradaic constant (96485 C mol^{-1}), Q_{total} is integrated charge at each applied potential and R is ideal gas constant (8.314 J·mol^{-1} K^{-1}).

The liquid products were collected at the end of each electrolysis, and quantitative analysis was performed using an ion chromatograph (IC, Dionex Aquion). A series of calibration curves of standard HCOONa solutions were used to determine the concentration of $HCOO^-$ from its IC peak area. The FEs of $HCOO^-$ were calculated based on the Equation (2):

$$FE_{HCOO^-}\ (\%) = \frac{Z \times F \times n_{HCOO^-}}{Q\text{total}} \times 100\% \qquad (2)$$

where n_{HCOO^-} is the measured amount of $HCOO^-$ (in moles), t is the reaction time, Z is the number of electrons transferred, F is the faraday constant (96485 C mol^{-1}) and Q_{total} is integrated charge at each applied potential.

The $HCOO^-$ production rate (r_{HCOO^-})was calculated using the following Equation (3):

$$r_{HCOO^-}\ (\text{mmol cm - 2 h - 1}) = \frac{c \times V}{t \times S \times 1000} \qquad (3)$$

where c is the measured concentration of $HCOO^-$, V is the volume of cathode electrolyte, t is the reaction time, and S is the geometric area of the work electrode.

2. Additional data

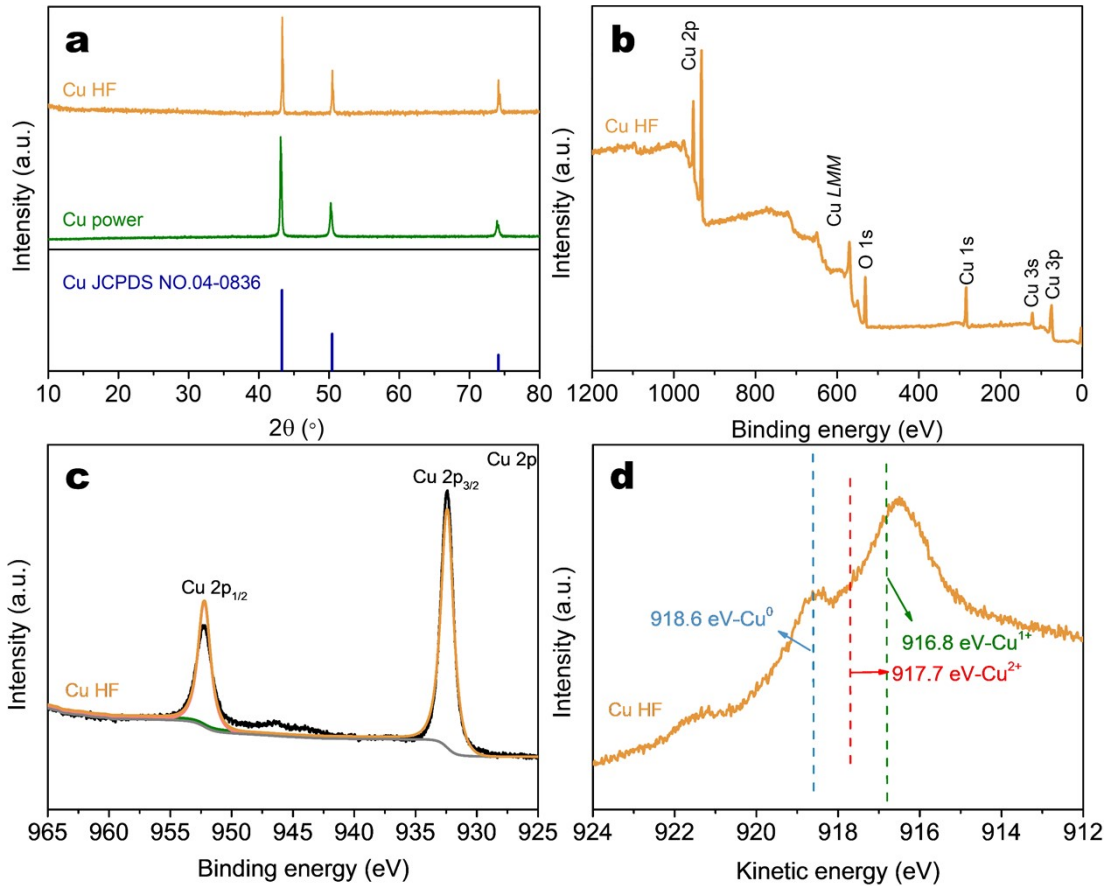

Fig. S1 (a) XRD pattern of Cu power and Cu HF. (b) Survey, (c) Cu 2p, and (d) Cu LMM Auger XPS spectra of Cu HF.

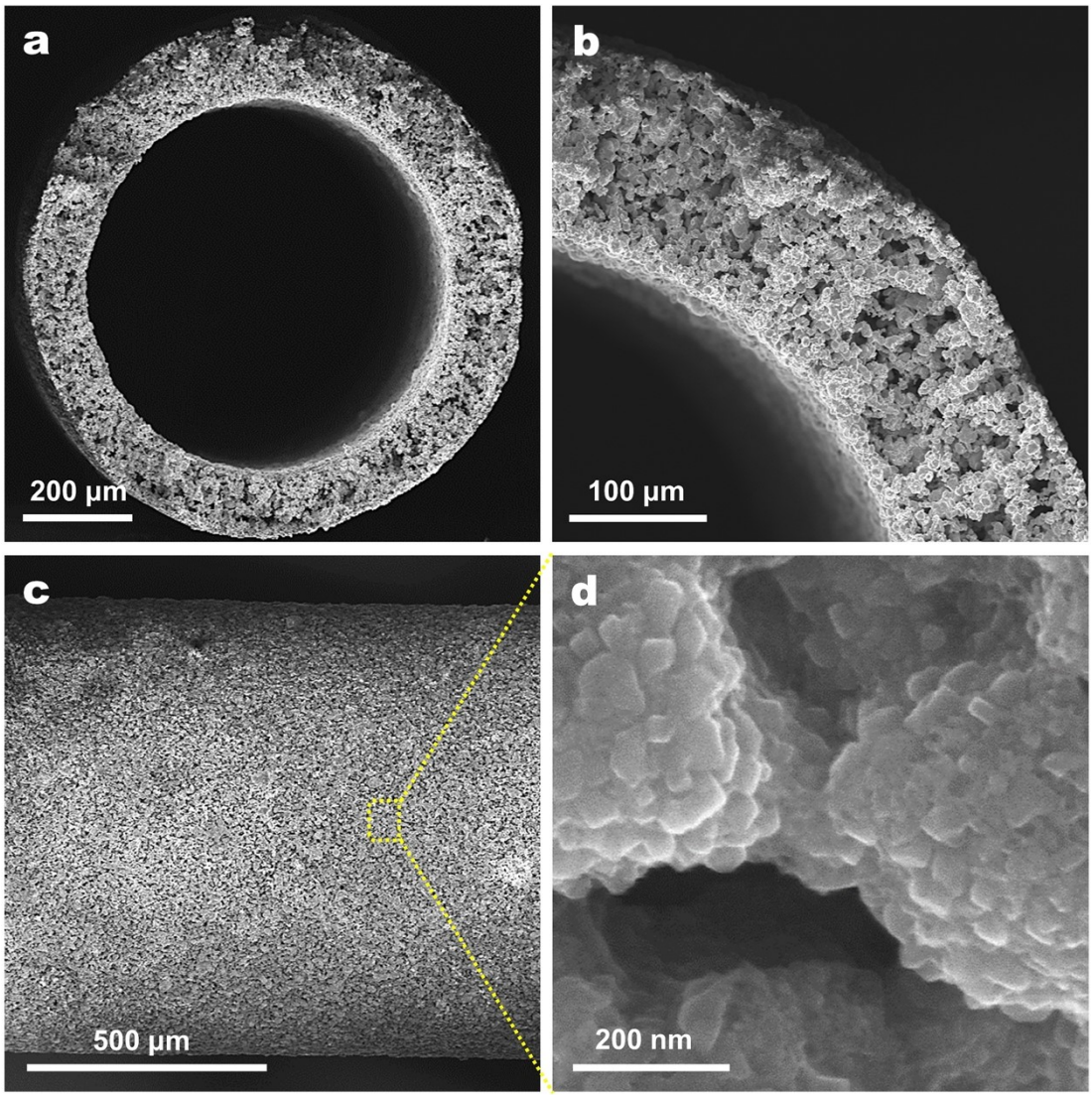

Fig. S2 SEM images of (a and b) cross-section and (c and d) outer surface of Cu HF.

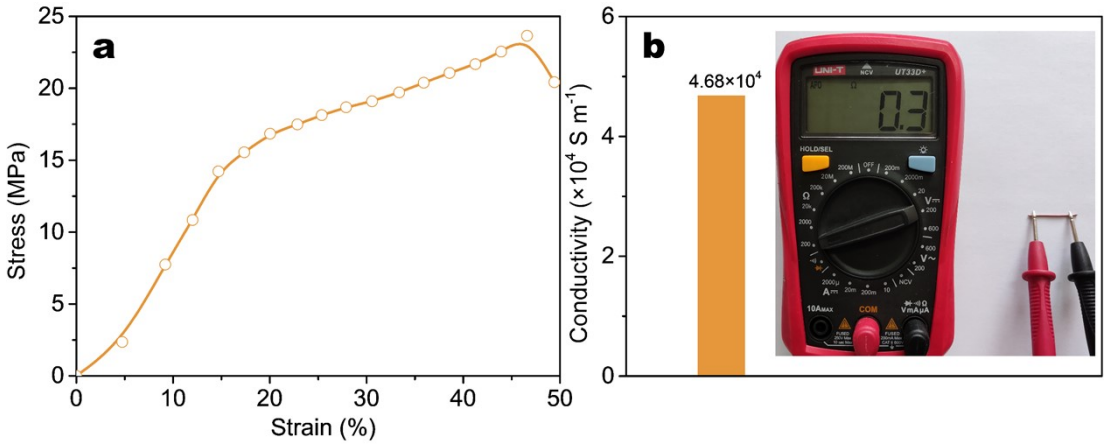

Fig. S3 (a) Stress-Strain curve and (b) electrical conductivity of the Cu HF GPE.

The as-fabricated Cu HF electrode can withstand a stress of 23.6 MPa at 46% tensile strain and the Youngs modulus reaches 118.7 MPa in the tensile stain range of 5% to 15%, demonstrating the excellent mechanical strength and ensuring the direct use of the Cu HF as a binder-free and self-supported electrode/host for either the CO_2RR or the growth of other electrochemical active species.

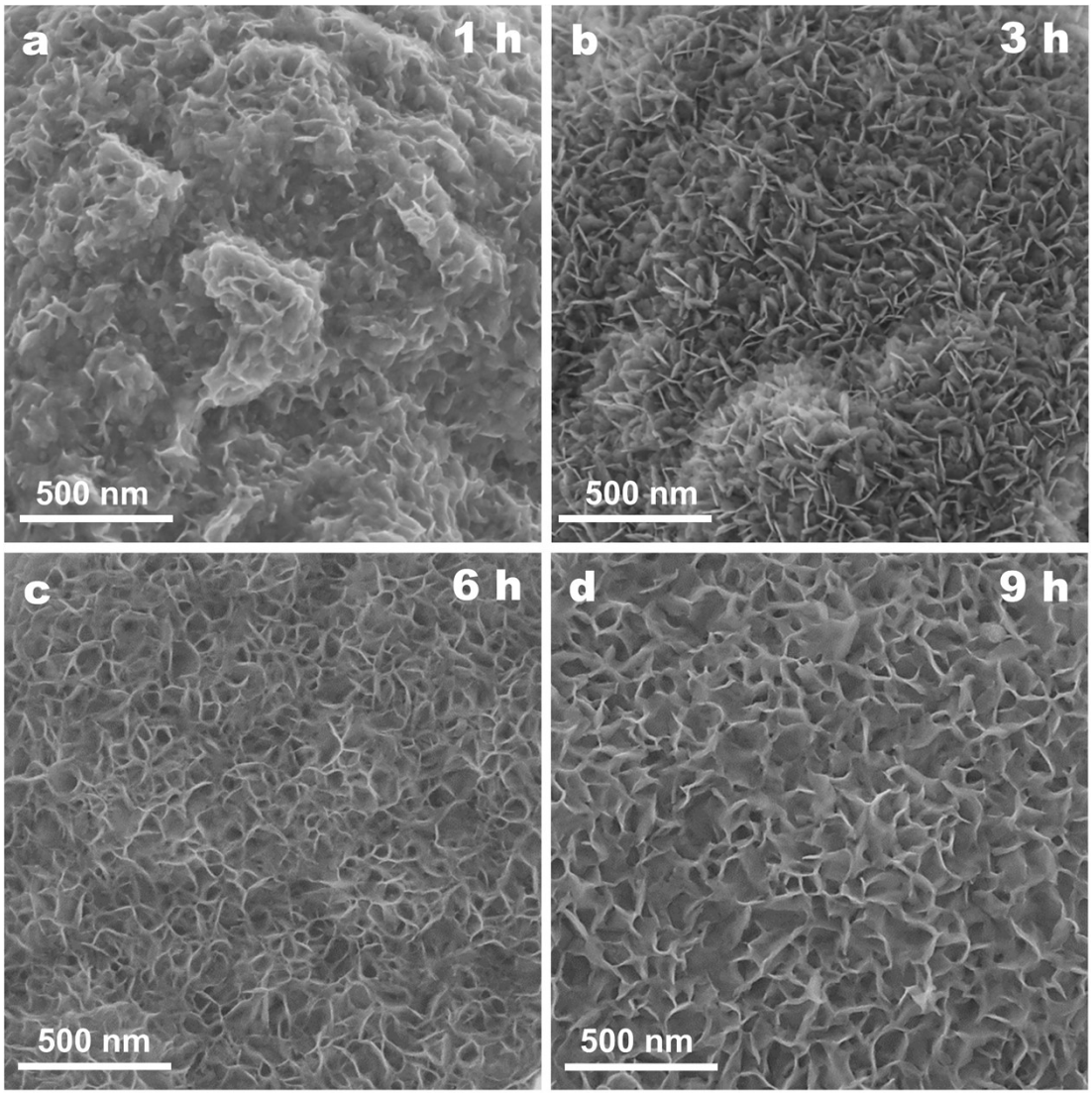

Fig. S4 SEM images showing the morphology evolution of grown Bi NSAs on Cu HF with the GRR time.

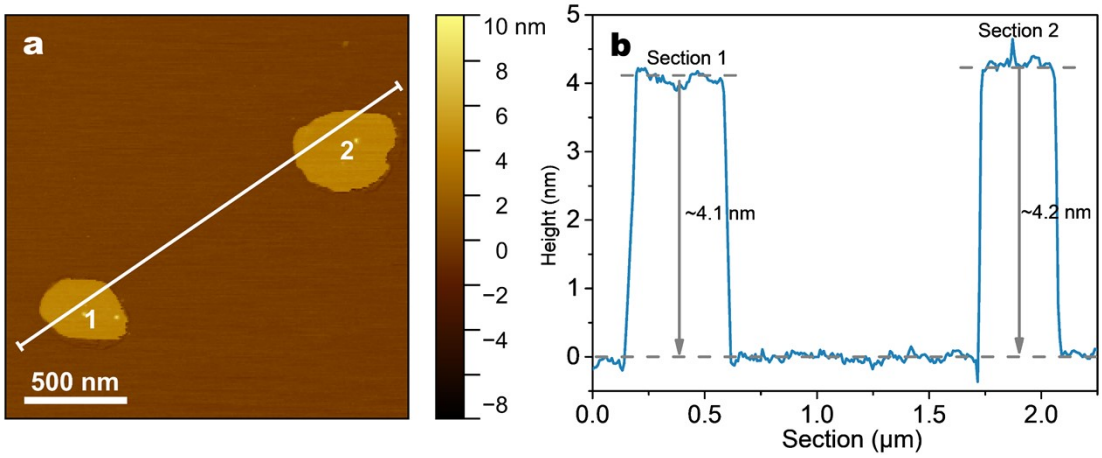

Fig. S5 (a) AFM image and (b) the corresponding height profile of Bi NSAs.

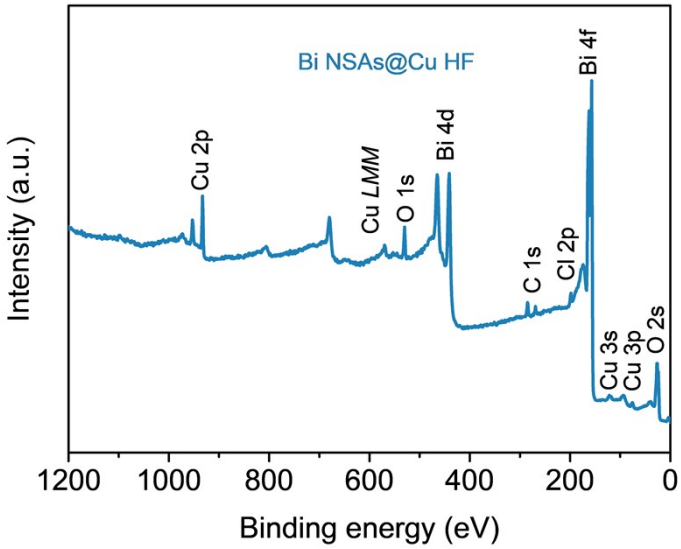

Fig. S6 XPS survey spectrum of Bi NSAs@Cu HF.

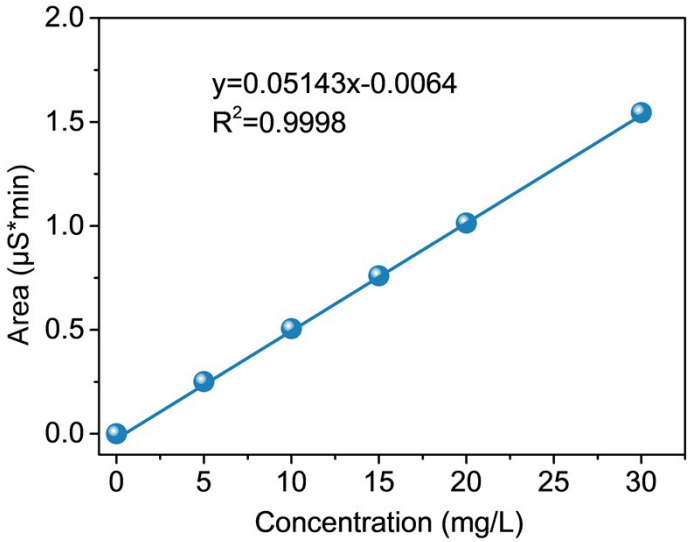

Fig. S7 Standard curve of peak area and concentration of $HCOO^-$.

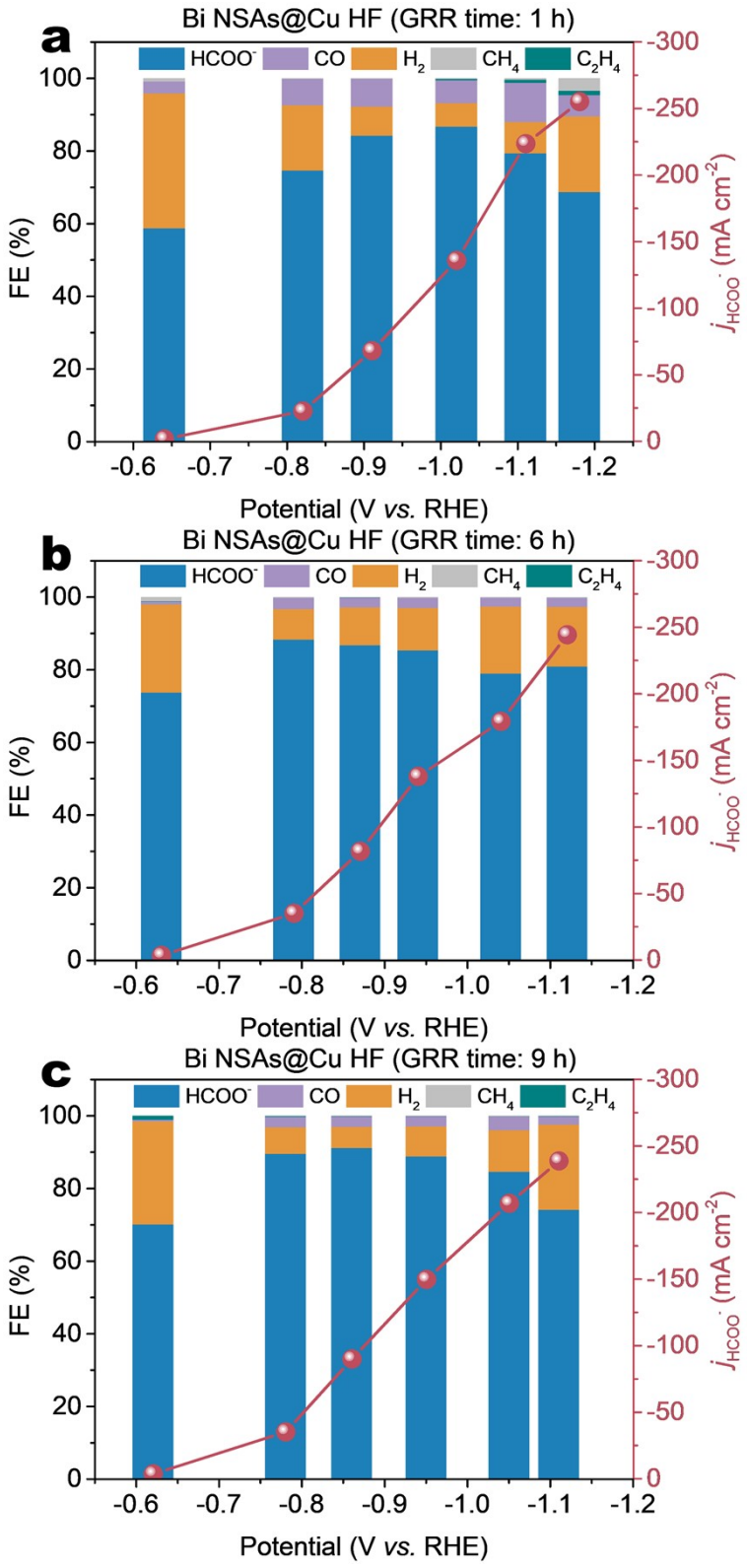

Fig. S8 FEs of CO_2RR products and partial current densities of $HCOO^-$ production for Bi NSAs@Cu HF GPEs prepared with different GRR times.

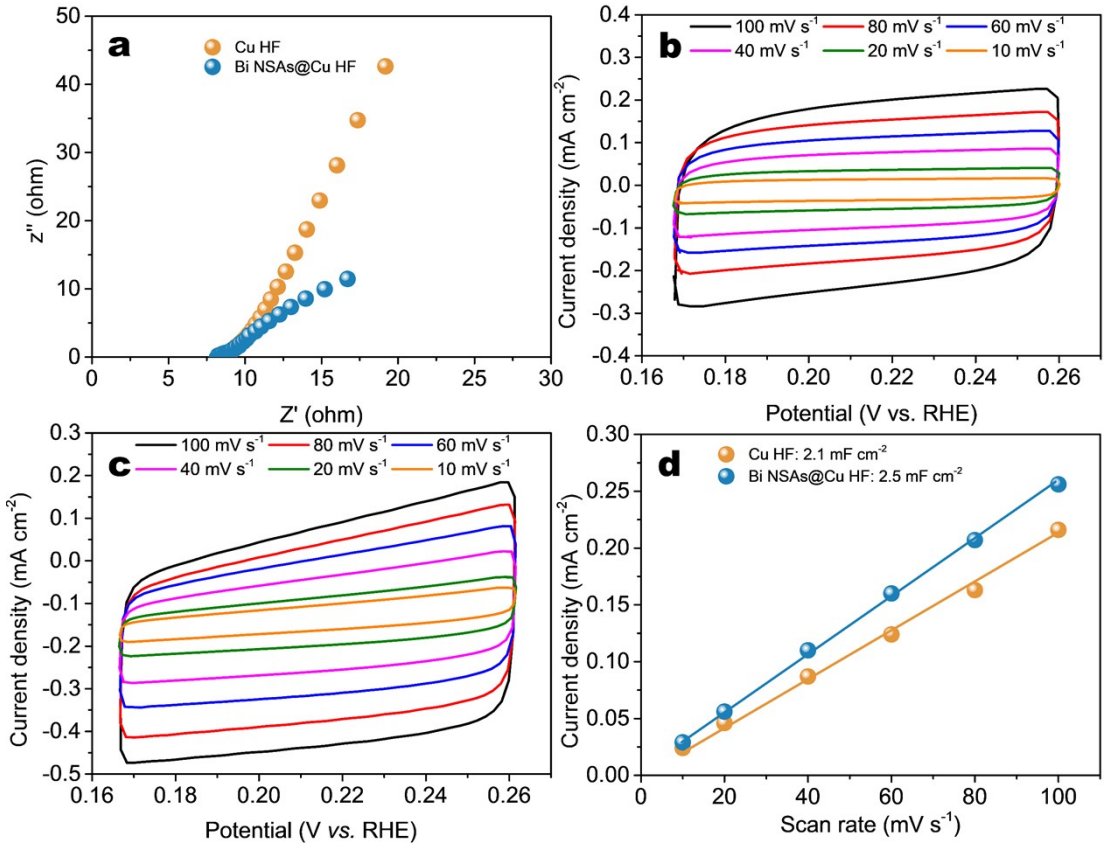

Fig. S9 (a) ElS curves of Cu HF and Bi NSAs@Cu HF GPE. CV curves of (b) Cu HF and (c) Bi NSAs@Cu HF GPE in the non-Faradaic region capacitance at different scan rates. (d) Current density plotted against scan rate for Cu HF and Bi NSAs@Cu HF GPE.

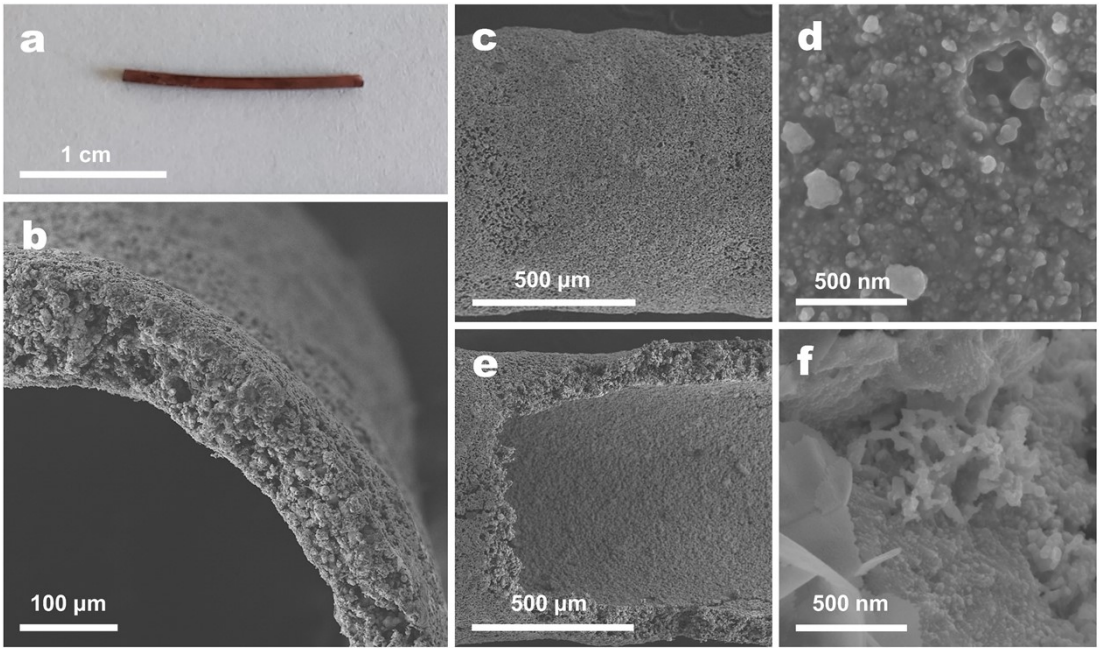

Fig. S10 (a) Optical photo, SEM images of (b) cross-section, (c and d) outer surface, and (e and f) inner surface of Bi NSAs@Cu HF GPE after CO_2RR stability test.

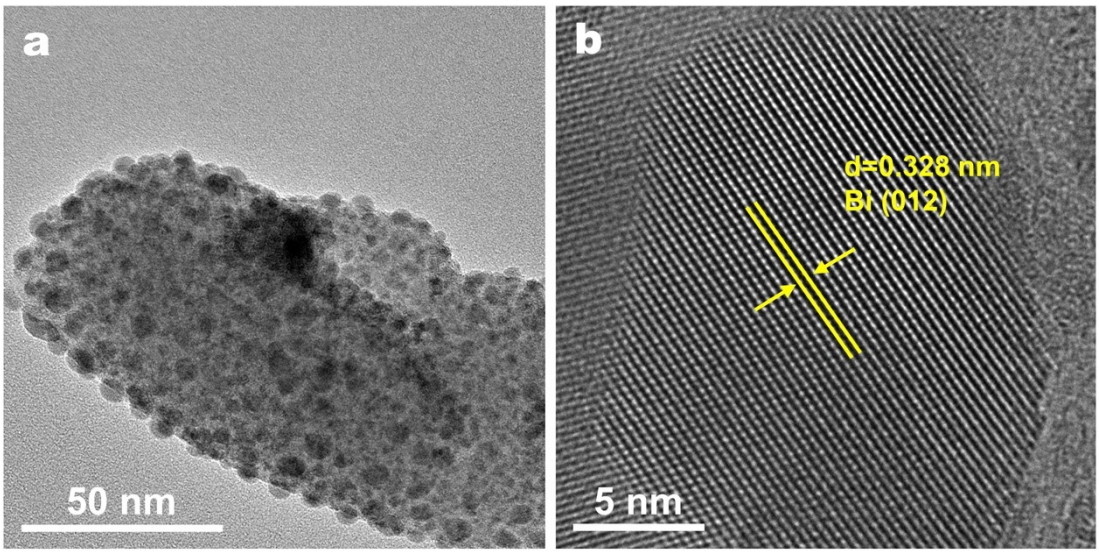

Fig. S11 (a) TEM and (b) HRTEM images of Bi NSAs@Cu HF GPE after CO_2RR stability test.

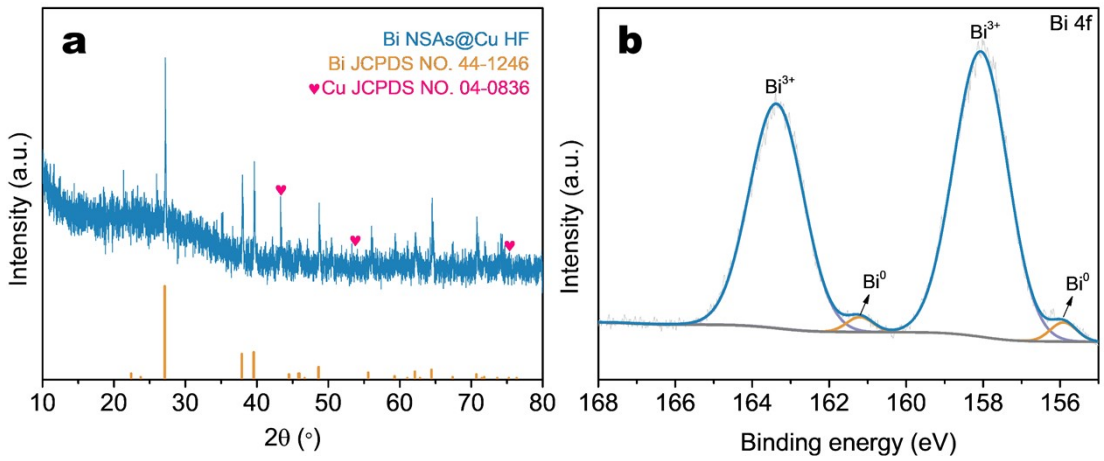

Fig. S12 (a) XRD pattern of Bi NSAs@Cu HF GPE and (b) Bi 4f XPS spectrum of Bi NSAs@Cu HF after CO_2RR stability test.

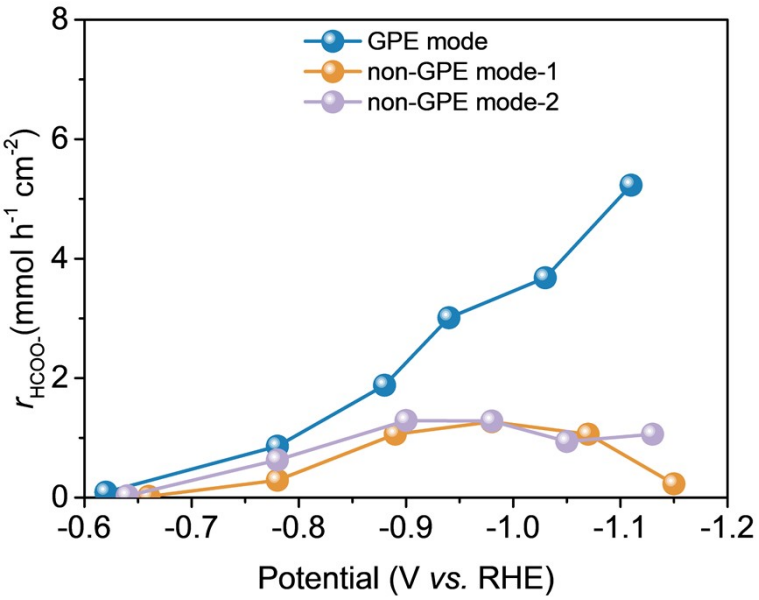

Fig. S13 $HCOO^-$ production rate for Bi NSAs@Cu HF electrode under different CO_2 transport modes.

Table S1 CO_2RR performance comparison of our Bi NSAs@Cu HF GPE in an H-type cell with other Bi-based electrocatalysts in H-type cells, flow cells, and MEAs for $HCOO^-$ production.

Catalyst	Reactor	Electrolyte	Potential (V *vs.* RHE)	FE_{HCOO^-} (%)	j_{HCOO^-} (mA cm^{-2})	Ref
Bi NAs	H-type cell	0.5 M $KHCO_3$	-0.95	90	-45	2
Cu-Bi	H-type cell	0.5 M $KHCO_3$	-1.0	92.5	-49.5	3
CuBi Catalyst	H-type cell	0.5 M $KHCO_3$	-1.5	90	-18	4
Bi-Cu Bimetallic	H-type cell	0.5 M $KHCO_3$	-0.91	94.37	-27.85	5
CuBi Bimetallic	H-type cell	0.5 M $KHCO_3$	-0.97	94.4	-38.5	6
Cu foam@Bi NW	H-type cell	0.5 M $KHCO_3$	-0.69	95	-15	7
Bismuthene@BP	H-type cell	0.5 M $KHCO_3$	-0.58	99	-54	8
Bi-ene-NW	H-type cell	0.5 M $KHCO_3$	-1.17	92	-88	9
Bi NS	H-type cell	0.5 M $KHCO_3$	-1.17	91	-25	10
Zn-Bi_3	H-type cell	0.5 M $KHCO_3$	-0.8	90	-20	11
BiOI-100	H-type cell	0.5 M $KHCO_3$	-0.9	90	-12	12
Bi Nanosheets	H-type cell	0.1 M $KHCO_3$	-1.0	90	-13	13
NTD-Bi	Flow cell	1 M $KHCO_3$	-0.85	95	-136	14
BiOBr	Flow cell	2 M $KHCO_3$		90	200	15
BiGDEs	Flow cell	0.5 M KCl+0.45 M $KHCO_3$	-1.2	90	-90	16
Bi NSs	Flow cell	1 M $KHCO_3$	-1.05	91	-98	17
S-$BiVO_4$	Flow cell	1 M $KHCO_3$	-1.0	95	-105	18
Bi/C NPs	MEA	0.5 M $KHCO_3$	3.0 (cell voltage)	90	-45	19
$CuBi_2O_3$-PE	H-type cell	0.5 M $KHCO_3$	-1.0	85	-141	20
CNT-Bi	H-type cell	0.5 M $KHCO_3$	-1.0	90	-148	21
Bi NSAs@Cu HF	H-type cell	0.5 M $KHCO_3$	-1.11	78.4	-261.6	This work

Supplementary references

1. C. Zhu, Y. Song, X. Dong, G. Li, A. Chen, W. Chen, G. Wu, S. Li, W. Wei and Y. Sun, *Energy Environ. Sci.*, 2022, **15**, 5391-5404.
2. J. Fan, X. Zhao, X. Mao, J. Xu, N. Han, H. Yang, B. Pan, Y. Li, L. Wang and Y. Li, *Adv. Mater.*, 2021, **33**, 2100910.
3. Z. Li, B. Sun, D. Xiao, Z. Wang, Y. Liu, Z. Zheng, P. Wang, Y. Dai, H. Cheng and B. Huang, *Angew. Chem. Int. Ed.*, 2023, **62**, e202217569.
4. M, Zu, L, Zhang, C, Wang, L Zheng and H, Yang, *J. Mater. Chem. A*, 2018, **6**, 16804-16809.
5. L, Peng, Y Wang, Y Wang, N Xu, W Lou, P Liu, D Cai, H Huang and J Qiao, *Appl. Catal. B*, 2021, **288**, 120003.
6. W Lou, L. Peng, R. He a, Y. Liu and J. Qiao, *J. Colloid Interface Sci.*, 2022, **606**, 994-1003.
7. X. Zhang, X. Sun, S. Guo, Alan M. Bond and J Zhang. *Energy Environ. Sci.*, 2019, **12**, 1334-1340.
8. F. Yang, A. Elnabawy, R, Schimmenti, P. Song, J. Wang, Z Peng, S. Yao, R. Deng, S. Song, Y. Lin, M Mavrikakis and W. Xu. *Nat. Commun.*, 2020, **11**, 1088.
9. M. Zhang, W. Wei, S Zhou, D Ma, A Cao, X. Wu and Q. Zhu, *Energy Environ. Sci.*, 2021, **14**, 4998-5008.
10. D. Wu, X Shen, J. Liu, C. Wang, Y. Liang, X. Fu and J. Luo, *Nanoscale*, 2019, **11**, 22125-22133.

11. T. Zhang, Y. Qiu, P. Yao, X. Li and H. Zhang, *ACS Sustain. Chem. Eng.*, 2019, **7**, 15190-15196.

12. D. Wu, J. Liu, Y. Liang, K. Xiang, X. Z. Fu and J. L. Luo, *ChemSusChem*, 2019, **12**, 4700-4707.

13. M. Zhao, Y. Gu, W. Gao, P. Cui, H. Tang, X. Wei, H. Zhu, G. Li, S. Yan, X. Zhang and Z. Zou, *Appl. Catal. B*, 2020, **266**, 118625.

14. Q. Wang, C. Zhu, C. Wu and H. Yu, *Electrochimica Acta*, 2019, **319**, 138-147.

15. F. P. García de Arquer, O. S. Bushuyev, P. De Luna, C. T. Dinh, A. Seifitokaldani, M. I. Saidaminov, C. S. Tan, L. N. Quan, A. Proppe, M. G. Kibria, S. O. Kelley, D. Sinton and E. H. Sargent, *Adv. Mater.*, 2018, **30**, 1802858.

16. G. Díaz-Sainz, M. Alvarez-Guerra, J. Solla-Gullón, L. García-Cruz, V. Montiel and A. Irabien, *J. CO2 Util.*, 2019, **34**, 12-19.

17. J. Yang, X. Wang, Y. Qu, X. Wang, H. Huo, Q. Fan, J. Wang, L. M. Yang and Y. Wu, *Adv. Energy Mater.*, 2020, **10**, 2001709.

18. W. Ma, J. Bu, Z. Liu, C. Yan, Y. Yao, N. Chang, H. Zhang, T. Wang and J. Zhang, *Adv. Funct. Mater.*, 2020, **31**, 2006704.

19. G. Díaz-Sainz, M. Alvarez-Guerra, B. Ávila-Bolívar, J. Solla-Gullón, V. Montiel and A. Irabien, *Chem. Eng. J.*, 2021, **405**, 126965.

20. H. Rabiee, L. Ge, X. Zhang, S. Hu, M. Li, S. Smart, Z. Zhu and Z. Yuan, *Appl. Catal. B*, 2021, **286**, 119945.

21. H. Rabiee, L. Ge, J. Zhao, X. Zhang, M. Li, S. Hu, S. Smart, T. E. Rufford, Z. Zhu, H. Wang and Z. Yuan, *Appl. Catal. B*, 2022, **310**, 121362.